

Supplementary Materials

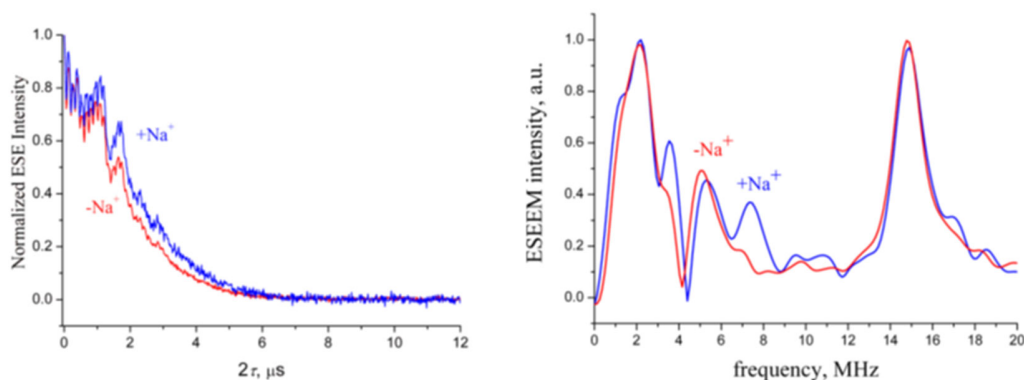


Figure S1. (left) Two-pulse echo decay traces of flavin radicals in the sodium (red line) and sodium-free (blue line) Na^+ -NQR samples. The traces were taken at the constant magnetic field B_0 , corresponding to the maximum of EPR spectra, at 80 K. The microwave pulse sequence was $\pi/2 - \tau - \pi - \tau - \text{echo}$, with duration of π -pulse 32 ns.

(right) Absolute value Fourier Transform spectra of the 2 pulse ESEEM of flavin radicals in the sodium (blue line) and sodium-free (red line) Na^+ -NQR samples (data from left). The spectra were normalized to the maximal intensity. The frequencies of the additional peaks for sodium sample (3.7 MHz and 7.4 MHz) are close to Zeeman and double Zeeman frequencies of ^{23}Na nuclei at $B_0 = 3470$ G (3.9 MHz and 7.8 MHz, respectively). "Adapted with permission from reference S1. Copyright 2012 American Chemical Society."

Section S1. ^{14}N ESEEM and HYSCORE.

The ESEEM experiments detect nuclear frequencies of the magnetic nuclei interacting with the unpaired electron. For ^{14}N , the nuclear spin $I = 1$ results in six nuclear frequencies where two single-quantum (sq) and one double-quantum (dq) transitions correspond to each electron spin manifold. However, some of these transitions could be formally forbidden and have a negligible intensity in the spectra of oriented systems. This phenomenon depends upon the strength of nuclear Zeeman, hyperfine and quadrupole interactions, and their relative orientation in the g -tensor coordinate system.

In orientation-disordered systems, an additional factor influencing the intensity of the different transitions is their orientation dependence. Strong orientation dependence of some transitions often prevents the appearance of observable lines with otherwise well-pronounced maxima. For a concrete illustration of the features appearing in orientation-disordered 1D and 2D spectra from ^{14}N nucleus, one can consider its interaction with $S = 1/2$ spin described by arbitrary of the isotropic hyperfine constant, a , nuclear Zeeman frequency, $\nu_{^{14}\text{N}}$, and nuclear quadrupole tensor with the principal values $(2K, -K(1+\eta), -K(1-\eta))$, where $K = e^2qQ/4h$ is the quadrupole coupling constant

and η is the asymmetry parameter. The q and Q are defined as the electric field gradient and the nuclear quadrupole moment, respectively, while h is Plank's constant. The ^{14}N nucleus can produce up to six lines in an ESEEM spectrum. Because of the variable dependence on orientation, not all transitions contribute equally to the spectra of powder samples. The ESEEM spectrum expected from ^{14}N with predominantly isotropic hyperfine coupling is governed by the ratio of effective nuclear frequencies determining the local magnetic field at two projections of the electron spin, $\nu_{eff\pm} = |\nu_{14\text{N}} \pm a/2|$, to the value of K [S2].

When $\nu_{eff\pm} < 1$, the splitting of three nuclear spin transitions in a corresponding manifold will be dominated by the nuclear quadrupole resonance frequency of ^{14}N , as defined by the principal values of the quadrupole tensor. They are independent of the direction of the magnetic field and give rise to three narrow peaks in the ESEEM spectra at

$$\nu_+ = K(3 + \eta) \quad \nu_- = K(3 - \eta) \quad \nu_0 = 2K\eta \quad (\text{S1})$$

with the property $\nu_+ = \nu_- + \nu_0$. The best condition for the observation of this triplet (eq.(S1)) is the so-called *cancellation* condition, when $\nu_{eff\pm} \approx 0$ or $\nu_{14\text{N}} \approx |a/2|$.

If $\nu_{eff\pm} > 1$, a single line without pronounced orientation dependence is expected from each corresponding manifold. This line is produced by a transition at the maximum frequency, which is a double-quantum transition $\nu_{dq\pm}$ between the nuclear spin states with $m_I = -1$ and 1. The frequency of this transition is described by eq. (S2) [S2],

$$\nu_{dq\pm} = 2[\nu_{eff\pm}^2 + K^2(3 + \eta^2)]^{1/2} \quad (\text{S2})$$

Two other single-quantum ($\nu_{1sq\pm}$ and $\nu_{2sq\pm}$) transitions involving $m_I = 0$ usually do not show any resolved peaks because of the significant orientation dependence of the quadrupole interaction. Reported ^{14}N ESEEM and HYSCORE spectra for $S = 1/2$ usually present one of two cases: 1) $\nu_{eff} < 1$ in one manifold and $\nu_{eff} > 1$ in another manifold; 2) $\nu_{eff} > 1$ in both manifolds. In case 1, the three-pulse ESEEM spectrum will present four lines, with three frequencies arising from the manifold with $\nu_{eff} < 1$ (described by eq. S1), and a fourth corresponding to ν_{dq} from the manifold with $\nu_{eff} > 1$. NQR frequencies give K and η , which characterize the chemical type of the ^{14}N nitrogen and its electronic state, while the ν_{dq} frequency provides the hyperfine coupling. In case 2, the three pulse ESEEM spectrum consists of two lines corresponding to frequencies ν_{dq-} and ν_{dq+} . Observation of these two lines allows calculation of the hyperfine coupling as

$$a = (v_{dq+}^2 - v_{dq-}^2) / (8v_{14N}) \quad (S3)$$

as well as the determination of $K^2(3 + \eta^2)$, which provides an estimate of K , suggesting variation of η between 0 and 1.

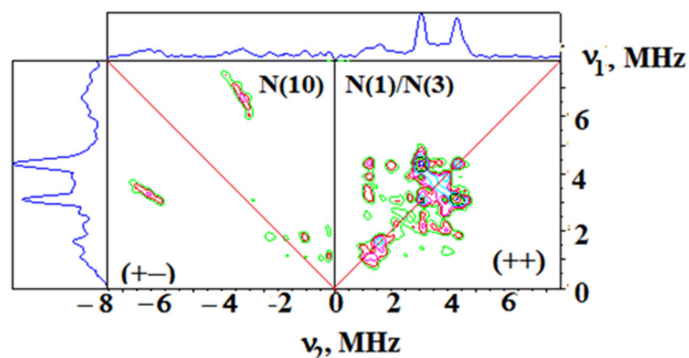


Figure S2. HYSCORE spectrum of the **anionic** flavin radical in the dithionite reduced Na^+ -NQR at temperature 100 K, MW frequency was 9.700 GHz, magnetic field 346 mT ($g=2.003$).

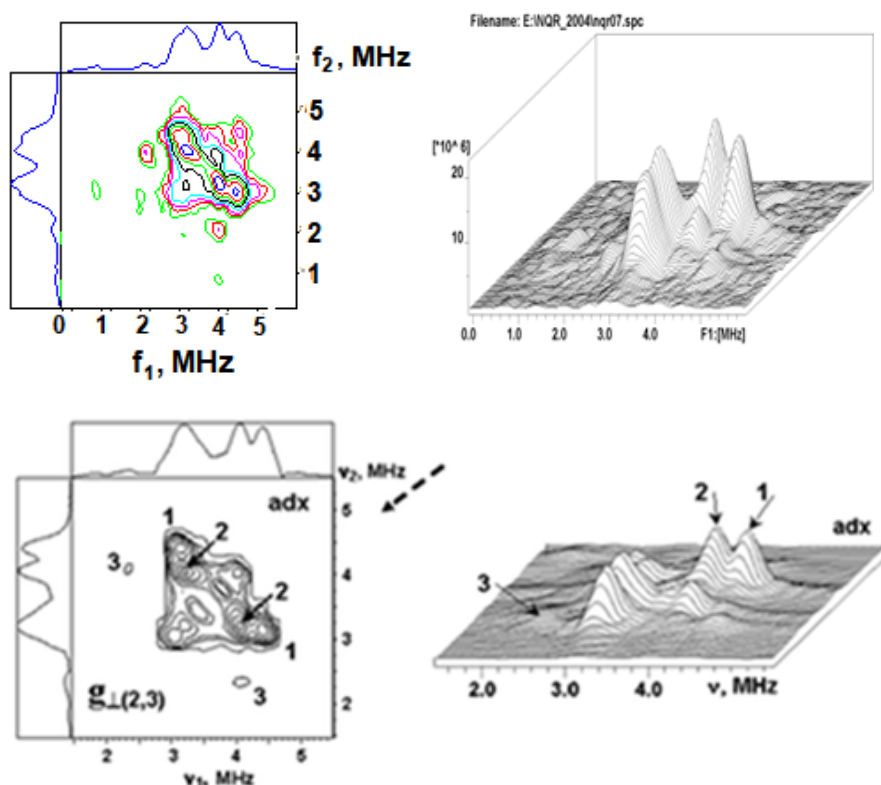


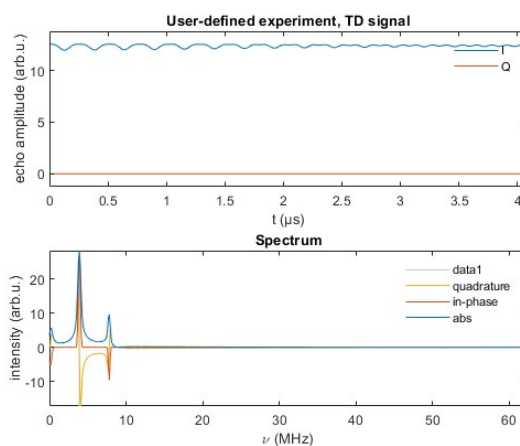
Figure S3. The contour (left) and stacked (right) presentations of ^{14}N HYSCORE spectra of the reduced $[2\text{Fe-2S}]$ cluster in the NQR (top) and adrenodoxin (bottom). Both spectra measured near $g_{2,3(\perp)} = 1.935$ at the fields 359.0 mT, the time τ between first and second microwave pulses is equal to 136 ns for both spectra. Arrows indicate the direction from which the 3D stacked perspective is viewed. Adrenodoxin spectra adapted by permission from Copyright Clearance Center: RSC Publishing, Dikanov et al. [S3]. Copyright 2009.

Table S1. Atomic magnetic hyperfine constants

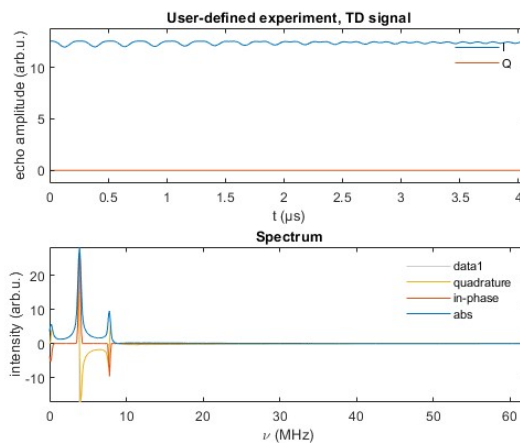
	¹ H	¹³ C	¹⁴ N	Refs.
<i>a</i> , MHz	1422.7 ^a	3333	1540	S4
		3777	1811	S5
<i>T</i> , ^c MHz		234.7	178.1	S4
		268.5	194.3	S5

^aExperimental, ^bRecalculated from the values reported for ¹⁴N [S4, S5], using multiplication coefficient 1.4. ^cMaximum component of the anisotropic hyperfine tensor can be estimated by multiplying values of *T* in the table with the angular factor 4/5 for *p* orbitals and −4/7 for *d* orbitals.

5 Å



4.5 Å



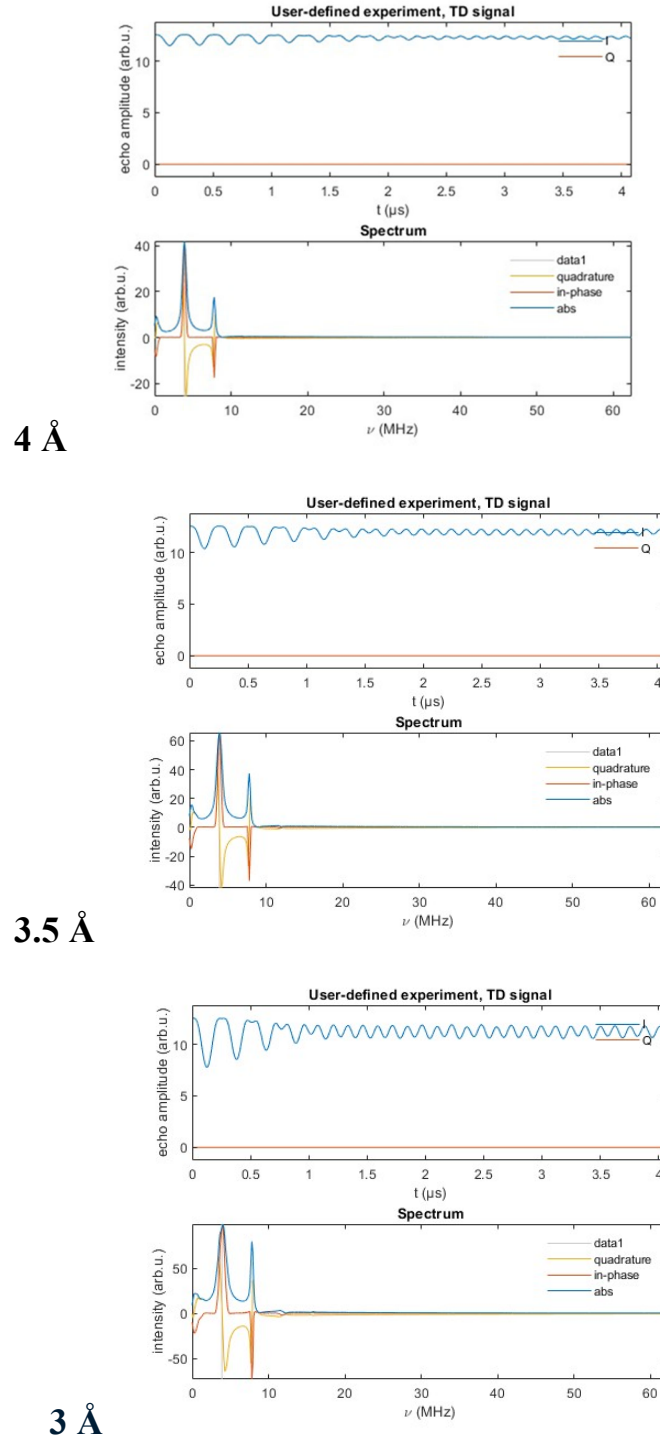


Figure S4. Two-pulse ^{23}Na ESEEM in the time and frequency domains simulated in the point dipole approximation for distances from 5 Å (top) to 3 Å (bottom) with a step of 0.5 Å between the unpaired electron and the ^{23}Na nucleus. Simulated spectra show that the ratio of peak intensities of the ν_{Na} and $2\nu_{\text{Na}}$ lines in these spectra increasing at smaller distances and varies from 0.81 for 3 Å to 0.29 for 5 Å (**Figure 5**). This result suggests that the preferred effective distance between the electron and the $^{23}\text{Na}^+$ nucleus in dipole-dipole approximation is $\sim 3\text{--}3.5$ Å.

Table S2. Hyperfine Coupling Matrices (Principal Values in MHz) and g-Matrices for the Neutral and Anionic Flavin Radicals in Na⁺-NQR Used in Simulations of X-band and W-band Spectra (Uncertainties in Parentheses)^{a‡}

	A _x	A _y	A _z	α ^a	β ^a	γ ^a
Neutral Radical						
¹⁴ N(5) ^b	0.2 (10)	0.2 (10)	52.5 (5)	45 (5)	7 (3)	
¹⁴ N(10)	2.0 (10)	2.0 (10)	28.9 (6)	12 (5)	13 (3)	
N(5)H	0.2 (10)	38.6 (6)	25.8 (6)	8 (5)	5 (3)	0 (3)
C(1')H	8.1 (10)	9.3 (10)	8.4 (8)	8 ^f	5 ^f	0
C(8α)H	10.0 ^c	8.5 ^c	8.5 ^c	8 ^f	5 ^f	−60
C(6)H	1.4 ^d	5.4 ^d	6.0 ^d	8 ^f	5 ^f	30
W ^e	3.59	4.27	3.04	8 (5)		
G	2.004 25 (2)	2.003 60 (2)	2.002 27 (2)			
Anionic Radical						
¹⁴ N(5)	2.3 (6)	2.3 (6)	57.6 (5)	21 (5)	1 (4)	
¹⁴ N(10)	1.6 (6)	1.6 (6)	22.8 (6)	1 (5)	6 (4)	
N(5)H						
C(1')H	7.4 (8)	5.0 (8)	4.5 (6)	36 (5)	0	0
C(8α)H	11.9 ^c	10.0 ^c	10.0 ^c	36 ^g	0	−60
C(6)H	4.4 ^d	8.9 ^c	8.9 ^c	36 ^g	0	30
W ^e	4.49	2.09	3.48	54 (5)		
G	2.004 36 (2)	2.004 02 (2)	2.002 28 (2)			

^{a‡}Adapted with permission from reference S6. Copyright 2003 American Chemical Society."

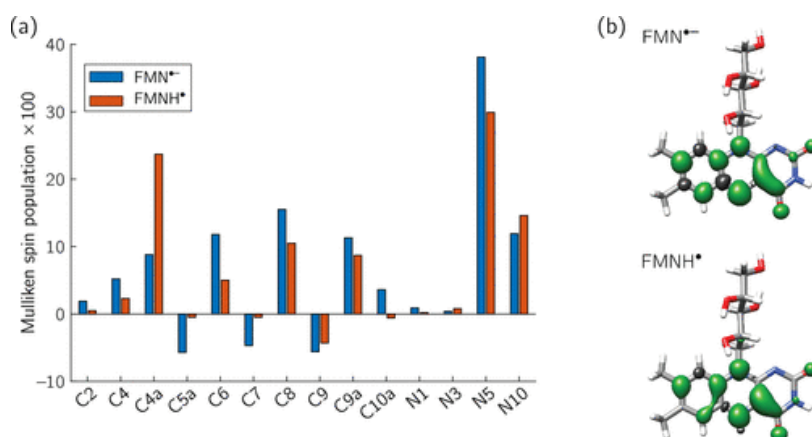


Figure S5. (a) Bar chart visualization of the Mulliken spin population analysis for the isoalloxazine ring atoms of FMN obtained from DFT calculations (B3LYP/EPR-II) for both protonation species. All numerical values are summarized in Table S8 of ref. S7. (b) Spin density surface plot for FMN•⁻ and FMNH• as obtained from DFT calculations (B3LYP/EPR-II). Spin density plots were created by using the

UCSF Chimera visualization software. "Adapted with permission from reference S7. Copyright 2022 American Chemical Society."

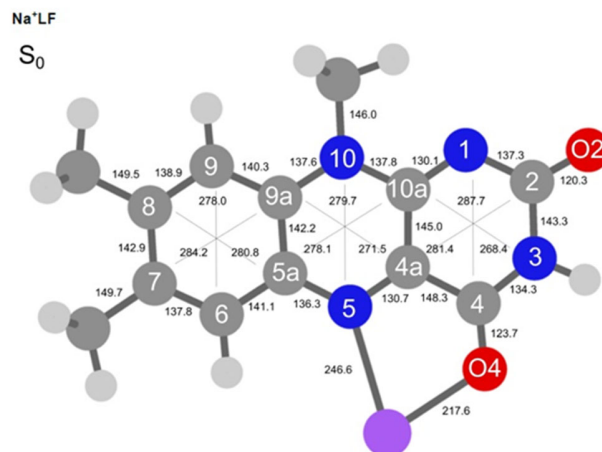


Figure S6. (Top) Absolute distances (in pm) of Na^+ LF in its S_0 state calculated at the PBE0/cc-pVDZ level.1q. "Adapted with permission from reference S8. Copyright 2019 the Royal Society of Chemistry."



Figure S7. Crystal structure of the *Geobacillus zalihae* T1 lipase (PDB code: 2DSN). Na^+ is depicted as a dark blue sphere. A close-up view of the configuration of the catalytic site is also shown (right panel). In the active site, Na^+ is coordinated to the side chains of Phe16, Ser113, and His358. " Adapted with permission from S9. Copyright 2009 American Chemical Society."

References.

- S1. Verkhovsky, M.I.; Bogachev, A.V.; Pivtsov, A.V.; Bertsova, Y.V.; Fedin M.V.; Bloch, D.A.; Kulik L.V. Sodium-Dependent Movement of Covalently Bound FMN Residue(s) in Na^+ -Translocating NADH: Quinone Oxidoreductase. *Biochemistry* **2012**, *51*, 5414-5421.
- S2. Dikanov, S.A.; Tsvetkov, Yu.D.; Bowman, M.K.; Astashkin, A.V. Parameters of quadrupole coupling of ^{14}N nuclei of chlorophyll *a* cations determined by electron spin echo method. *Chem. Phys. Lett.* **1982**, *90*, 149-153.
- S3. Dikanov, S.A.; Samoilova, R.I.; Kappl, R.; Crofts A.R.; Hüttermann, J. The reduced [2Fe-2S] clusters in adrenodoxin and *Arthrospira platensis* ferredoxin share spin density with protein nitrogens, probed using 2D ESEEM. *Phys. Chem. Chem. Phys.* **2009**, *11*, 6807 – 6819.
- S4. Fitzpatrick, J.A.J.; Manby, F.R.; Western, C.M. *J. Chem. Phys.* **2005**, *122*, 084312.

S5. Morton, J.R.; Preston, K.F. Atomic parameters for paramagnetic resonance data. *J. Magn. Reson.* **1978**, *30*, 577-582.

S6. Barquera, B.; Morgan, J.; Lukoyanov, D.; Scholes, C.P.; Gennis, R.B.; Nilges, M.J. X- and W-Band EPR and Q-Band ENDOR Studies of the Flavin Radical in the Na⁺-Translocating NADH: Quinone Oxidoreductase from *Vibrio cholerae*. *J. Am. Chem. Soc.* **2003**, *125*, 265–275.

S7. Pompe, N.; Illarionov, B.; Fischer, M.; Bacher, A.; Weber, S. Completing the Picture: Determination of ¹³C Hyperfine Coupling Constants of Flavin Semiquinone Radicals by Photochemically Induced Dynamic Nuclear Polarization Spectroscopy. *J. Phys. Chem. Lett.* **2022**, *13*, 5160–5167.

S8. Müller, D.; Nieto, P.; Miyazaki, M.; Dopfer, O. Effect of alkali ions on optical properties of flavins: Vibronic spectra of cryogenic M⁺ lumiflavin complexes (M=Li-Cs) *Faraday Discuss.* **2019**, *217*, 256-275.

S9. Hagiwara Y.; Matsumura H.; Tateno M. Functional roles of a structural element involving Na⁺- π interactions in the catalytic site of T1 lipase revealed by molecular dynamics simulations. *J Am Chem Soc.* **2009**, *131*, 16697–16705.

;